Authentication of Medicines Using Nuclear Quadrupole Resonance Spectroscopy

Cheng Chen, Fengchao Zhang, Jamie Barras, Kaspar Althoefer, Swarup Bhunia, and Soumyajit Mandal

Abstract—The production and sale of counterfeit and substandard pharmaceutical products, such as essential medicines, is an important global public health problem. We describe a chemometric passport-based approach to improve the security of the pharmaceutical supply chain. Our method is based on applying nuclear quadrupole resonance (NQR) spectroscopy to authenticate the contents of medicine packets. NQR is a non-invasive, non-destructive, and quantitative radio frequency (RF) spectroscopic technique. It is sensitive to subtle features of the solid-state chemical environment and thus generates unique chemical fingerprints that are intrinsically difficult to replicate. We describe several advanced NQR techniques, including two-dimensional measurements, polarization enhancement, and spin density imaging, that further improve the security of our authentication approach. We also present experimental results that confirm the specificity and sensitivity of NQR and its ability to detect counterfeit medicines.

Index Terms—Medicines authentication, counterfeit medicines, NQR, nitrogen

1 Introduction

Access to safe medicines is a human right recognized by the United Nations (U.N.) In 2013, the U.N. Human Rights Council (UNHCR) adopted a resolution on access to medicines that stressed "the responsibility of States to ensure access to all, without discrimination, of medicines, in particular essential medicines, that are affordable, safe, effective and of good quality" [1]. However, there is a growing illicit trade in medicines that undermines attempts to ensure safe access [2], [3], [4]. In particular, falsified or substandard medicines with altered or non-existent APIs (active pharmaceutical ingredients) are widespread in the pharmaceutical supply chain, particularly in low- and middle-income countries (LMICs) with weak pharmacovigilance and drug regulatory systems [5]. Globally, antimicrobials and antimalarials are two of the classes of medicines most targeted by counterfeiters [5]. For example, a nationwide sample survey in 2008 found that 12.2 percent of antimalarials at retail outlets in Tanzania were of poor quality [6]. Such altered drugs are not only directly dangerous to human health, but can also cause resistance to the genuine drug to develop over time.

The extent of the counterfeit medicine problem can be judged from a sampling of published reports related to the People's Republic of China (PRC). In inspections carried out by the Shanghai Food and Drug Administration (FDA) in 2006 and 2007, 3.5 and 4.5 percent, respectively, of medicines tested were found to be of poor quality. In 2012, the *Shanghai Daily* reported that 1,900 people were detained and fake drugs worth U.S. $182 million were seized in a nationwide crackdown. The problem is particularly acute with Traditional Chinese Medicine (TCM): in 2011, the same newspaper reported that a third of TCM ingredients tested in Guangdong province failed quality tests; in 2012, 25.5 percent of TCM samples tested by the Hubei province FDA failed these tests. Similar quality control problems have been detected in other countries. For example, during Operation Pangea VII in 2014, Interpol seized 9.4 million doses of "fake" and "illicit" medicines seized worldwide *within one week*. Tens of millions of illicit medicines are now seized every year at various E.U. borders. These goods account for 20 percent of all illicit goods seized, and about 63 percent of them enter the E.U. via the postal system. Such trade is estimated to be worth $12.8 billion per year.

Counterfeit medicines may contain the correct APIs, the wrong APIs, no APIs, or insufficient APIs. Substandard medicines also do not contain the correct amount of API or have altered API bioavailability, but this is due to poor quality control at point of manufacture or degradation during storage rather than deliberate fraud. The most common method of authenticating medicines is still visual inspection of the packaging and contents. Several technological approaches are also being developed. The Falsified Medicines Directive (FMD) recently adopted by the E.U. means that by 2018 all packaged medicines transported into and across the E.U. will need:

1) An unique medicines identifier (UMI), i.e., a different reference number for every packet (not just every brand or batch).
2) A tamper-evident seal. Packets with broken seals would not continue down the supply chain.

The problem is that UMI-based "track and trace" approaches, such as RFID tags, authenticate the packet, *not the contents*. They are thus vulnerable to the "seal of approval" trap, in which people assume that a packet is

- *C. Chen and S. Mandal are with the Department of Electrical Engineering and Computer Science, Case Western Reserve University, Cleveland, OH 44106. E-mail: {sxm833, cxc717}@case.edu.*
- *F. Zhang and S. Bhunia are with the Department of Electrical and Computer Engineering, University of Florida, Gainesville, FL 32611. E-mail: {fxz67, skb21}@case.edu.*
- *J. Barras and K. Althoefer are with the Department of Informatics, King's College, London, United Kingdom. E-mail: Jamie.Barras@kcl.ac.uk, kaspar.althoefer@kcl.ac.uk.*

Manuscript received 1 Sept. 2015; revised 8 Dec. 2015; accepted 14 Dec. 2015. Date of publication 23 Dec. 2015; date of current version 1 June 2016. For information on obtaining reprints of this article, please send e-mail to: reprints@ieee.org, and reference the Digital Object Identifier below. Digital Object Identifier no. 10.1109/TCBB.2015.2511763

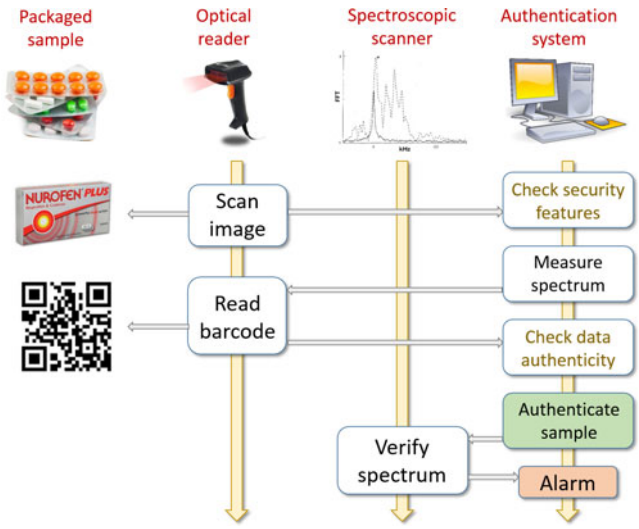

Fig. 1. Simplified flowchart of the chemometric passport-based approach for authenticating medicines proposed in this paper.

genuine simply because it has a security mark and so don't bother to check the code. We would like to develop an authentication approach that fits within the FMD framework (and similar efforts in other countries), but goes further by authenticating the actual contents of the packet. This approach should be applicable across the globe, in all territories affected by counterfeit and/or substandard medicines, and in a range of scenarios, from supply chain security to border customs control and medicine checks in hospitals. Proposed methods include *covert tagging* and several *chemical fingerprinting* techniques [7].

In this paper we describe an *chemometric passport* approach to solve this quality assurance problem. Chemometric data on packaged medicines will be derived from a spectroscopic analysis performed at the point of manufacture. The contents of the packet will later be authenticated by matching the results of another spectroscopic analysis with unique chemical identifiers (UCIs) from a reference spectrum. The latter will be accessed either from a secure database stored in the cloud, or from information encoded directly within the product barcode, as shown in Fig. 1. The absence of a match triggers a "contents don't match the label" alarm, which may be due to several underlying causes including intentional fraud, poor manufacturing practices, and degradation due to poor storage or being past the expiry date. Such chemometric authentication can be carried out at various stages of the medicine supply chain, such as during manufacturing, distribution, dispensing, and home use. It may also be possible to authenticate the product by comparing spectroscopic measurements with more basic identity information, such as the name of the manufacturer and brand, API, number and weight of pills/capsules within the packet, and the bill of lading. This capability would be particularly useful in applications where the barcode may not be visible, such as at customs checkpoints and postal sorting offices.

2 Theory

Nuclear Quadrupole Resonance (NQR) spectroscopy is a non-invasive and non-destructive analytical technique that is highly suitable as a chemometric passport for medicines [8], [9], [10], [11], [12]. About 50 percent of atoms in the periodic table contain so-called quadrupolar nuclei with spin quantum number $I \geq 1$ that generate NQR signals. Specifically, almost all medicines have APIs that contain NQR-active nuclei such as nitrogen (^{14}N) and chlorine (^{35}Cl). NQR is insensitive to pill coatings and non-metallic packaging material; it is particularly useful for examining packaged pills in bulk quantities (full bottles or complete blister packs), shipping cartons containing bottles or packs, and drums of loose material (powder). The required instrumentation is also *simple and low-cost* compared to other analytical techniques such as liquid chromatography, mass spectrometry, X-ray powder diffraction, and THz, Raman, infrared (IR), or near-infrared spectroscopy [13], [14], [15], [16]. Moreover, RF-based methods like NQR are inherently safe, emit no damaging radiation, and can be used without any protective clothing or special safety training. It is therefore highly suitable for authentication of pharmaceuticals by end-users without any specialized knowledge. Much of the prior work on NQR-based authentication of pharmaceutical products was performed in Europe. For example, the CONPHIRMER consortium was funded by the E.U. to create a portable, easy-to-use sensor to detect packaged counterfeit medicines. This project, which was led by Kings College London, ended in December 2014 with the creation of a single prototype that could test two medicines, metformin and paracetamol, and was field-tested to a limited extent at Warsaw Airport by the Polish Customs Service.

2.1 NQR Physics

NQR spectra are generated by resonant transitions between nuclear energy levels created by the interaction between the electric quadrupole moments of certain nuclei and their local electric field gradient tensor (EFG). Only nuclei with spin quantum numbers $I1$ are "quadrupolar", i.e., have the asymmetric charge distributions required to generate non-zero quadrupole moments and thus NQR spectra [17]. The resultant resonances occur in the radio frequency (RF) part of the electromagnetic spectrum, as shown in Fig. 2. For example, ^{14}N ($I = 1$) and ^{35}Cl ($I = 3/2$) resonances typically occur in the 0.1-5 MHz and 20-40 MHz ranges, respectively. We will focus on ^{14}N since it is the dominant isotope (99.635 percent abundance) of nitrogen, which in turn is present within most APIs.

An external static magnetic field is not required for NQR spectroscopy, unlike the related technique of nuclear magnetic resonance (NMR). Thus NQR is sometimes referred to as "zero-field NMR". However, it is limited to materials in the solid state, unlike NMR.

The nuclear Hamiltonian, or total energy operator, assumed during NQR experiments is given by

$$H_Q = \frac{\omega_Q}{3}\left[3I_z^2 - I(I+1) + \frac{\eta}{2}\left(I_+^2 + I_-^2\right)\right]. \quad (1)$$

Here ω_Q is known as the quadrupolar coupling constant, $0 \leq \eta \leq 1$ is known as the asymmetry parameter of the EFG tensor in the principal axis system (PAS) fixed on the nucleus, and I_z, I_+, and I_- are known as spin operators. The corresponding energy levels and transitions between them are shown in Fig. 3 for the two most common cases, $I = 1$ and

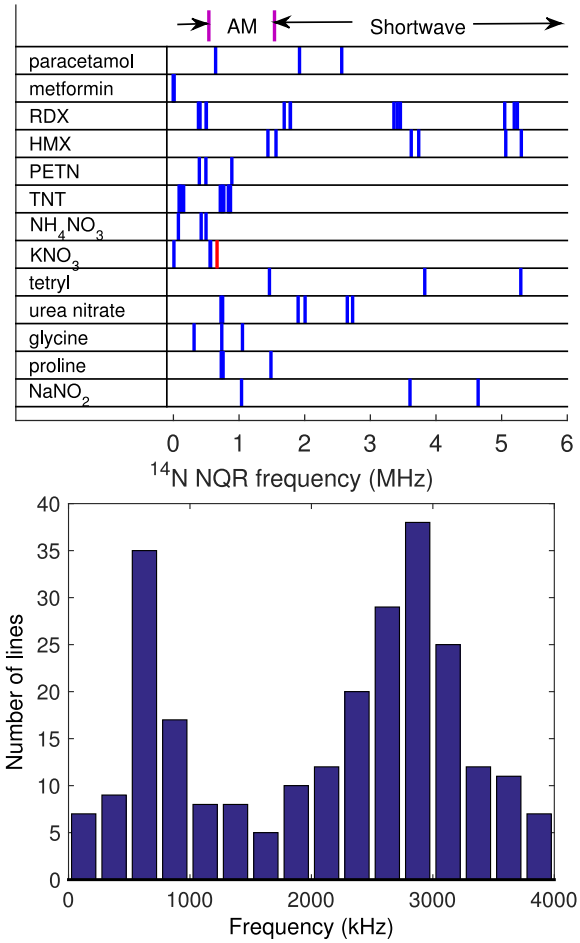

Fig. 2. Top: ^{14}N NQR lines of several compounds, including common medicines, explosives, and amino acids (blue lines), and the ^{39}K NQR line of potassium nitrate (red line). Bottom: Histogram showing the distribution of ^{14}N NQR frequencies in 45 different medicines and their polymorphs (data from Kings College London, the Josef Stefan Institute, and the University of Ljubljana, Slovenia) [18]. The frequencies span the entire range from 0 to 4 MHz, with peaks around 650 and 2,850 kHz.

3/2. There are three energy levels and resonance frequencies (traditionally denoted by ω_+, ω_-, and ω_0) for $I = 1$, as follows:

$$\omega_\pm = \frac{3\omega_Q}{4}\left(1 \pm \frac{\eta}{3}\right), \qquad \omega_0 = \omega_+ - \omega_- = \frac{\eta\omega_Q}{2}. \tag{2}$$

Similarly, there are two doubly-degenerate levels and a single resonant frequency for $I = 3/2$:

$$\omega_0 = \frac{\omega_Q}{2}\sqrt{1 + \frac{\eta^2}{3}}. \tag{3}$$

The latter degeneracy can be removed by an external magnetic field. For a particular nucleus, the parameters ω_Q and η define the transition frequencies. These parameters depend on the local electric field distribution, which is a sensitive function of molecular structure, i.e., static properties of the crystal lattice. Moreover, the widths of these transitions are sensitive to molecular motion, i.e., dynamic properties of the lattice.

As a result, NQR resonance frequencies are highly specific to the chemistry of the material under investigation.

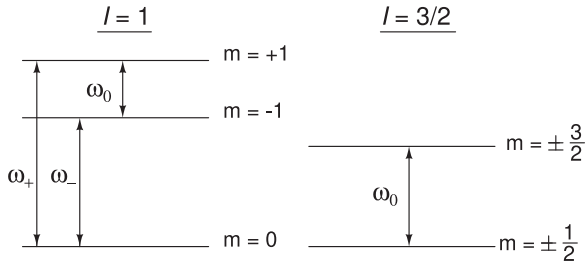

Fig. 3. Energy level diagrams and transition frequencies for quadrupolar nuclei with spin quantum numbers $I = 1$ and 3/2.

Other signal characteristics (amplitude, line width) provide additional information, such as the amount of material present, the physical form (e.g., polymorphs, ratios of stereoisomers, anhydrous or hydrated), physical processing (e.g., loose powder, pressed pill), and changes in material properties caused by aging and impurities [18], [19], [20]. The technique is so sensitive to the solid-state environment of molecules that it can even distinguish between the same pharmaceutical preparations from different manufacturers [20]. For example, measured NQR linewidth differences between several commercially available tablets of paracetamol (a common analgesic) were found to be a consequence of different compacting pressures used during production of the tablets [21]. This high degree of specificity to the physical and chemical properties of the material under investigation allows NQR spectra to be treated as *unique chemical fingerprints* or *physical one-way functions* [22].

Fig. 4 shows a simplified block diagram of an NQR-based medicines authentication system. From an abstract point of view, each quadrupolar nucleus can be viewed as a nonlinear dynamical system. NQR experiments are usually carried out by alternately perturbing a large number of such nuclei away from thermal equilibrium and detecting the sum of the resulting responses as they gradually return to equilibrium. This process is similar to that

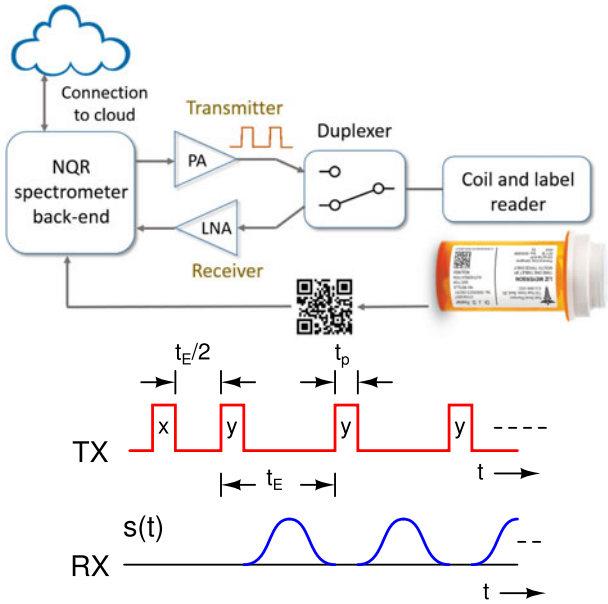

Fig. 4. Top: Simplified block diagram of an NQR-based medicines authentication system. PA = Power Amplifier, LNA = Low-Noise Amplifier. Bottom: Basic spin-locked spin echo (SLSE) pulse sequence used for NQR experiments, and the resulting received signal $s(t)$.

used in challenge-response authentication and is known as the pulsed or half-duplex mode of operation, as shown in Fig. 4. The resulting spin dynamics are complex nonlinear functions of multiple sample properties and excitation sequence parameters. *Such complexity makes it difficult for external sources to replicate NQR signals, which increases the security of this materials authentication approach.*

The perturbing signal (excitation) is known as a *pulse sequence*, i.e., consists of one or more RF pulses with frequency ω_{RF}, amplitude A, and relative phase ϕ that are generated by a high-power transmitter circuit. These pulses are applied to the sample by a transmitter coil that generates an oscillating magnetic field which is usually known as B_1. This field perturbs the populations of the nuclear energy levels from their values by inducing transitions between them when the resonance condition is satisfied, i.e., when ω_{RF} is close to one of the NQR transition frequencies. As a result, coherent superpositions of pure quantum states ("coherences" for short) are generated within each nucleus. These coherences oscillate with time in a manner that is controlled by the pulse sequence. The ensemble of such excited nuclei generates an oscillating magnetic dipole moment $M(t)$ within the sample. A macroscopic receiver coil converts this time-varying magnetization into an oscillating voltage $v(t) \propto dM(t)/dt$ through Faraday induction. In many systems the same physical coil is used for both transmission and reception; in this case a transmit/receive switch (duplexer) is used to control access to the coil. The detected voltage is amplified and digitized by a low-noise RF receiver circuit. The acquired NQR signal is further processed by a "back-end" to extract parameters of interest, such as signal amplitude, frequency, and phase. Modern back-ends are usually based on a programmable digital platform such as a field-programmable gate array (FPGA) or digital signal processor (DSP).

2.2 NQR Signal Characteristics

The most common pulse sequence used for NQR experiments is known as the spin-locked spin echo (SLSE) or pulsed spin-locking (PSL) sequence. It consists of an initial *excitation pulse* and a long train of *refocusing pulses* separated by the *echo period* t_E as shown in Fig. 4. These pulse categories have the same length t_p, but are denoted by x and y to emphasize a relative phase shift of $\pi/2$ between them. The signals generated by this sequence are known as spin echoes and are acquired during the gaps between adjacent refocusing pulses. The entire sequence is usually repeated several times with a wait time t_w between scans. The detected signals from these scans are then averaged together to improve the signal-to-noise ratio (SNR).

The amplitude of each spin echo is generally estimated by integrating the acquired echo signal $s(t)$ after it has been weighted with a known window function $w(t)$. Thus the amplitude of the kth echo is given by

$$a_k = \frac{\int_{-t_{acq}/2}^{+t_{acq}/2} s_k(t) w(t) dt}{\sqrt{\int_{-t_{acq}/2}^{+t_{acq}/2} |w(t)|^2 dt}}. \tag{4}$$

Here t_{acq} is the duration of the signal acquisition window. The variance of a_k, which determines the measurement uncertainty, is a function of unwanted components (noise and interference) within $s(t)$. The optimum window function $w_{opt}(t)$ for maximizing output SNR depends on noise properties. In the presence of additive white Gaussian noise, it is well-known that $w_{opt}(t) = s^*(t)$, i.e., the complex conjugate of the expected echo shape. This is known as the *matched filter*.

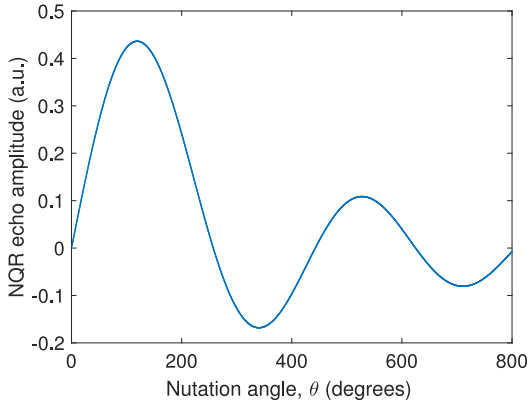

Fig. 5. Theoretical NQR response curve for powder samples containing spin $I = 1$ nuclei such as ^{14}N.

Echo amplitudes decrease with k, usually in a bi-exponential manner:

$$a_k = s_1 e^{-kt_E/T_{SLSE,1}} + s_2 e^{-kt_E/T_{SLSE,2}} + n_k. \tag{5}$$

Here the first two terms represent the NQR signal, while the third term (n_k) represents additive noise and interference. The amplitudes s_1 and s_2 are dependent on static sample properties (volume, density of nuclei, and crystal structure), geometry of the transmitter and receiver coils, and pulse sequence parameters (t_p, t_w, and ω_{RF}). In particular, they are directly proportional to the total number of active nuclei, which allows NQR to be used for quantitative analysis of mixtures. However, they are damped oscillatory functions of the strength of the excitation, which shows that the underlying dynamical system is strongly nonlinear. Excitation strength is usually quantified by the so-called nutation angle $\theta = \gamma |B_1| t_p$ of each RF pulse. Here γ is known as the gyromagnetic ratio and is constant for a given nuclear species, while $|B_1|$ is the amplitude of the RF magnetic field during each pulse. For polycrystalline (powder) samples with $\eta \neq 0$, it can be shown that the response function for both s_1 and s_2 is given by

$$s(\theta) = \sqrt{\frac{\pi}{2\theta}} J_{3/2}(\theta). \tag{6}$$

Here $J_{3/2}$ is the Bessel function of the first kind and order 3/2, and the maximum signal amplitude is obtained for a nutation angle of $\theta \approx 120°$. This function is plotted in Fig. 5; a slightly different one occurs in the special case when $\eta = 0$ [23]. The *relaxation time constants* $T_{SLSE,1}$ and $T_{SLSE,2}$ depend upon a different set of parameters, including dynamic sample properties (molecular motion) and the echo spacing t_E.

^{14}N NQR is a relatively insensitive measurement technique since the relevant energy level differences (and transition frequencies) are very small. Signal averaging over multiple scans is generally required to obtain an acceptable SNR. The resulting experimental time is limited by another sample-dependent relaxation time constant known as T_1.

Specifically, the detected signal amplitude increases exponentially with the inter-scan delay t_w as $1 - e^{-t_w/T_1}$, so long delays are required for samples with large values of T_1. These dependencies are exploited in state-of-the-art parametric signal models and algorithms for detecting NQR signals in the presence of noise and strong non-stationary interference [24], [25], [26].

The NQR signal can also be analyzed in the frequency domain. In this case many acquired echo signals $s_k(t)$ are summed up to increase SNR, as follows:

$$s_{av}(t) = w(t)\frac{\sum_{k=1}^{N_E} s_k(t) f(k)}{\sum_{k=1}^{N_E} |f^2(k)|}. \quad (7)$$

Here $f(k)$, which is known as an *apodization function*, weighs each echo by its expected SNR in order to maximize the SNR of the sum $s_{av}(t)$. It is therefore another example of a matched filter. An optimal choice for $f(k)$ is the expected signal decay function. For example, if the decay is mono-exponential with a time constant T_{SLSE}, $f_{opt}(k) = e^{-kt_E/T_{SLSE}}$. The value of T_{SLSE} may be obtained from prior knowledge, or by preliminary fitting of the measured decay function a_k. The average echo shape is weighted by a window function $w(t)$ to maximize SNR. The optimum choice of $w(t)$ in additive white noise is again the complex conjugate of the expected echo shape. Taking the Fourier transform of $s_{av}(t)$ finally results in the NQR spectrum $S_{av}(\omega)$ around the excitation frequency ω_{RF}.

The spectrum $S_{av}(\omega)$ contains narrowband features (lines) centered around the NQR resonance frequencies. Both the frequencies and widths of these lines contain information about the sample. However, the line widths measured using pulsed methods such as SLSE are broadened because of the limited time over which individual echoes can be acquired. In other words, $S_{av}(\omega)$ is the result of convolving the true NQR spectrum with the Fourier transform of the signal acquisition window, which has a spectral width of at least $1/t_E$. The echo spacing t_E can be increased to reduce such spectral broadening and improve the specificity of the measurement. However, increasing t_E usually causes T_{SLSE} to decrease and thus reduces SNR.

External RF interference (RFI) is a major concern for NQR measurements. Such interference is usually unintentional. For example, Fig. 2 shows that the broadcast AM radio band overlaps with the frequency range of ^{14}N NQR signals. However, RFI can also be intentionally created by attackers in order to disrupt the authentication process. Fortunately, NQR spin dynamics are complex and therefore difficult to replicate. Moreover, several techniques can be used to further increase robustness to such attacks.

2.3 Two-Dimensional (2D) Spectroscopy

Each ^{14}N atom (crystal site) in a molecule gives rise to resonance signals at three different frequencies, ω_+, ω_-, and ω_0, as shown in Fig. 2. The amplitudes of these signals are correlated since they originate from population differences between the same set of three nuclear energy levels. Compounds with several crystalline sites or a mixture of several compounds can exhibit a very broad and complex NQR spectrum with many resonance lines, which can be further contaminated by external RFI. As a result, it is often difficult to identify these resonance lines and thus quantify the composition of the sample. We have shown that population transfers between the correlated triplet lines that belong to the same crystalline site can be used to simplify the spectrum [27]. Such transfers use a single RF coil and a pulse sequence that contains pulses at two different frequencies, as shown in Fig. 6. The initial pulse (at frequency $\omega_{RF,1}$) changes the amplitude of the detected signal (at frequency $\omega_{RF,2}$) by predictable amounts while leaving any signals generated by other sites or by RFI unaffected. Four examples are shown in Fig. 6 for glycine (an amino acid). In three of these examples, the detected signal amplitude decreases when the frequency of the initial pulse matches one of the NQR resonances. In the fourth example, the signal amplitude increases. Both the sign and magnitude of these amplitude changes match theoretical predictions.

We have performed similar single-coil population transfer experiments on carbamazepine. This drug is sold under the tradename Tegretol among others, and is a medication used primarily for the treatment of epilepsy and neuropathic pain. The frequency of the initial pulse (f_1) was set to either of two NQR frequencies for this compound (3,876 or 3,829 kHz), and those of the other pulses (f_2) was set midway between the two (3,852 kHz) to allow simultaneous monitoring of the effect of the initial pulse on both transitions. The intensity of the f_2 transition was monitored with and without an initial saturation pulse (nominal nutation angle $\theta_1 = 90^\circ_{eff}$) or inversion pulse ($\theta_1 = 180^\circ_{eff}$) applied at f_1. Fig. 7 shows the measured spectra, and confirms that the detected signal intensity decreases significantly in both cases, as expected.

The two frequencies $\omega_{RF,1}$ and $\omega_{RF,2}$ can be systematically varied to build up a two-dimensional NQR spectrum [27]. In practice we usually plot the *difference spectrum*, i.e., the difference in signal intensity at each point with and without the initial RF pulse. The presence of off-diagonal peaks in this spectrum specifically identifies coupling between the corresponding transition frequencies, i.e., shows that they originate from the same crystal site. An experimental example is shown in Fig. 8.

One concern with full 2D measurements is experimental time, which may become prohibitively large for compounds with long values of T_1. A rapid version of the experiment, which is much faster than the full 2D version when the spectrum exhibits only a few lines of interest, has been proposed to solve this problem [27]. This technique was successfully used to identify the components of a binary mixture in the presence of substantial RFI. Spectrometers with several independent RF channels and coils allow even more sophisticated multi-dimensional NQR measurements. For example, they can implement pulse sequences based on simultaneous multi-frequency excitation [28], [29].

Changes in signal amplitudes due to population transfers are specific to the type of transition (ω_+, ω_-, or ω_0). They can thus be used to identify which lines in a ^{14}N spectrum belong to the same site. This is of particular relevance when there are clusters of lines arising from sites with only small differences in their quadrupolar parameters. A different method for analyzing complex NQR spectra is based on Zeeman shifts, i.e., resonant frequency and line shape changes of polycrystalline (powder) samples in

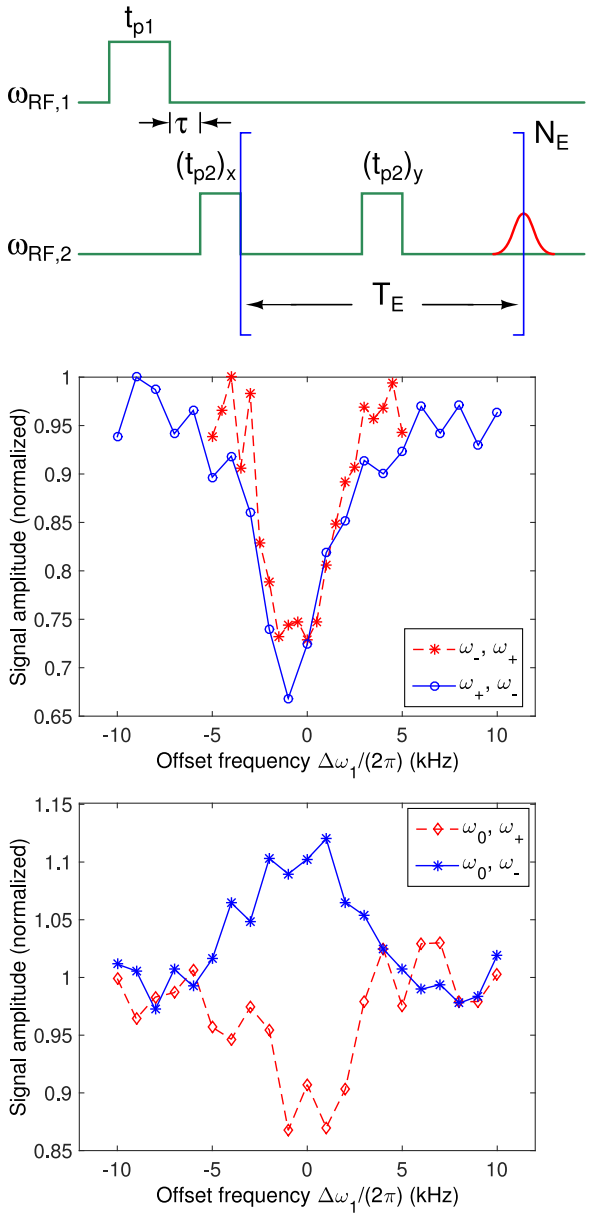

Fig. 6. Top: Two-frequency $(\omega_{RF,1}, \omega_{RF,2})$ pulse sequence with SLSE signal detection. The initial pulse is used to manipulate a second NQR transition at a different frequency, while the part within the brackets is repeated N_E times to obtain a train of spin echoes. The delay τ between the first and second pulses is kept short enough ($\tau \ll T_1$) to avoid longitudinal relaxation. A two-step phase cycle, in which the phases of the second pulse and the receiver are alternated between 0 and π, is normally used to cancel both static offsets in the electronics and ringing from the refocusing pulses. Middle and bottom: Measured NQR signal amplitudes for glycine powder with two-frequency excitation in four cases as a function of the first RF frequency. In all cases, the magnitudes and signs of the on-resonance amplitude changes match those predicted theoretically.

the presence of a small static magnetic field (B_0) [30]. The magnitude of these perturbations are also characteristic of the type of transition.

2.4 Polarization Enhancement

The weakness of NQR signals makes them vulnerable to corruption by RFI; this is often the limiting factor in real-world applications. Fortunately, signal strengths can be significantly enhanced by magnetization transfer (cross-

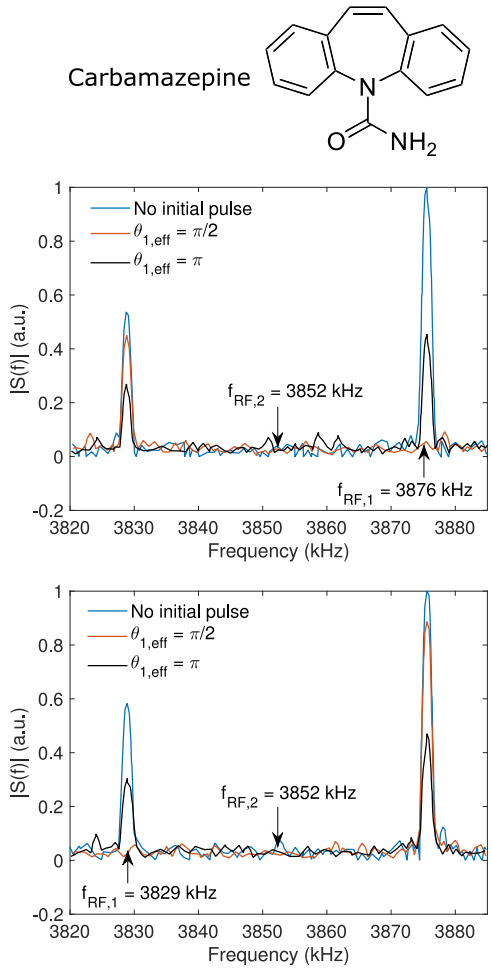

Fig. 7. Measured NQR spectra of carbamazepine using the two-frequency SLSE pulse sequence. The C-N(-C)-C site of this compound has $\omega_+ = 3,876$ kHz, $\omega_- = 3,829$ kHz, $\omega_Q = 5,134$ kHz, and $\eta = 0.02$. The coil used for these experiments was a 3 cm^3 solenoid, with $T_{90,eff} \approx 20\ \mu$s, and $T_{180,eff} \approx 50\ \mu$s at 3.8 MHz.

polarization) from other spins with larger gyromagnetic ratios, usually protons. Proton polarization can be created by placing the sample within a static magnetic field B_0. This field can be generated either by an electromagnet [31], [32] or a permanent magnet [33], [34]. The electromagnet is then either slowly turned off, or the sample mechanically

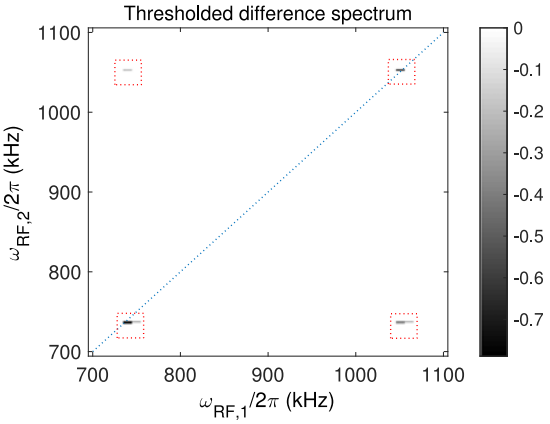

Fig. 8. Measured 2D NQR difference spectrum of glycine. The cross-peaks at 737 and 1,051 kHz show that these frequencies belong to a single site and correspond to the ω_+ and ω_- transitions, respectively [27].

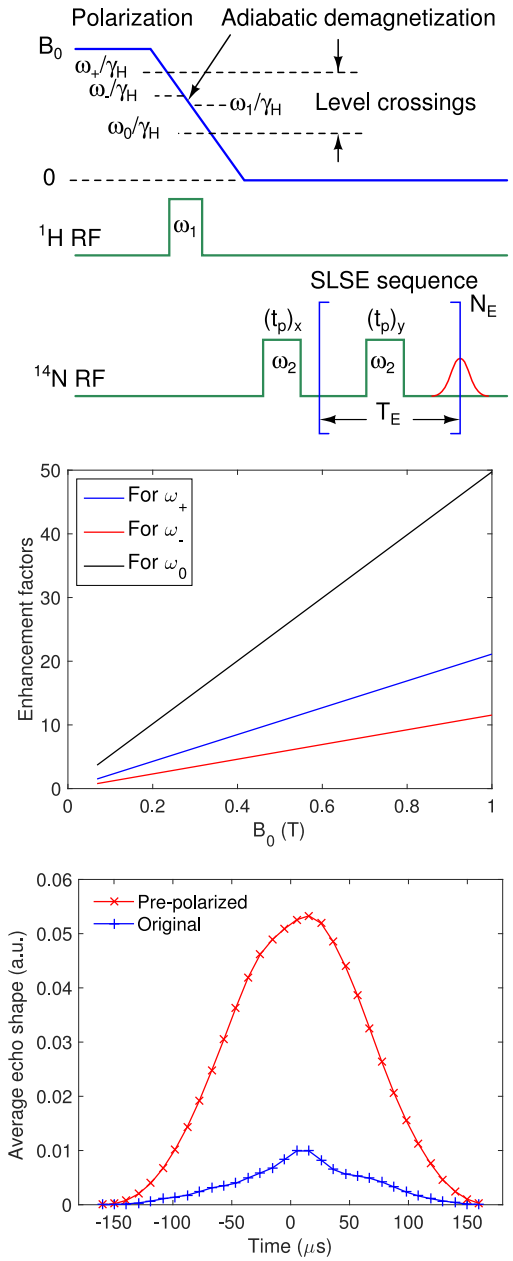

Fig. 9. Top: General scheme for polarization-enhanced NQR through ^{1}H-^{14}N level crossings. The demagnetization profile is digitally programmable through a sample motion controller and need not be linear as shown here. The enhanced NQR signal is detected through the common SLSE multi-echo pulse sequence. The ^{1}H RF pulse, which is optional, is used to control the relative enhancement of the NQR transitions by adiabatically inverting the proton polarization. Middle: Calculated signal enhancement factors for paracetamol (a common analgesic) as a function of polarization field strength. In practice, incomplete cross-polarization results in slightly lower enhancement factors. Bottom: Measured average NQR signal from the ω_+ transition (at 2.564 MHz) of paracetamol before and after pre-polarization with a 0.5 T static magnetic field. The sample consisted of 15 Tylenol caplets (500 mg each). Results are averaged over two scans (time = 30 sec) and show a signal enhancement factor of 6.7.

removed from the permanent magnet, resulting in adiabatic demagnetization and gradual decrease of the proton NMR frequency $\omega_L = \gamma_H B_0$.

Cross-polarization occurs during the demagnetization process when ω_L approaches any of the NQR frequencies; such events are known as *level crossings*. Three such level crossings can occur for each ^{14}N site, as shown in Fig. 6. The resulting "enhanced" NQR signals are detected outside the magnet (at zero field), which eliminates line broadening due to resonance frequency shifts and thus maintains the intrinsic frequency resolution of the measurement.

The amount of signal enhancement can be theoretically calculated. It depends on the type of NQR transition (ω_+, ω_-, or ω_0), initial field strength (B_0), and number of protons within each molecule. Fig. 9 shows that 6.7-fold increases in signal amplitude, corresponding to 45-fold decreases in averaging time, occur even in the relatively weak field ($B_0 = 0.5$ T) generated by a small permanent magnet. The field does not have to be particularly homogeneous, enabling the use of low-cost and easily-assembled designs, such as two-piece "shim-a-ring" magnets [35], [36]. Even portable low-power electromagnets can generate static fields that are strong enough (< 50 mT) to significantly enhance the amplitudes of low-frequency NQR resonances (< 1 MHz) [31]. A wide variety of polarization enhancement techniques can thus be implemented by adding both a permanent magnet with sample shuttle and a digitally-programmable electromagnet to the basic NQR spectrometer shown in Fig. 4. An additional RF transmitter is also useful. It can be used as a *proton channel*, i.e., to control the relative enhancement of the NQR transitions by adiabatically inverting the proton polarization during adiabatic demagnetization. An example is shown in Fig. 9.

Adding a permanent magnet and proton channel results in a fully-functional NMR spectrometer that is capable of performing a variety of relaxation and diffusion experiments that do not require a highly uniform magnetic field. The programmable electromagnet and sample shuttle are also useful for studying slow dynamics in many materials via the fast field-cycling (FFC) technique [37]. In particular, FFC can be used to indirectly detect ^{14}N NQR transitions by enhanced cross-relaxation of the protons. This effect shortens the longitudinal relaxation time constant T_1 near energy level-crossings. Such "quadrupolar dips" are often easy to detect, since the protons are polarized and detected at high field, i.e., within the permanent magnet, which results in high SNR. In addition, low-power electromagnets are sufficient since most ^{14}N NQR frequencies are lower than 3 MHz. However, such double resonance (DR) experiments have low spectral resolution because of Zeeman broadening of the quadrupolar transition. They are therefore most suitable for rapidly searching a broad frequency range for possible NQR transitions.

2.5 Stochastic Excitation

Broadband RF excitation is desirable in order to reduce the experimental time required to scan a given bandwidth for an NQR signal. The bandwidth of the excitation pulses shown in Fig. 4 is inversely proportional to their duration t_p, so the obvious solution is to use very short pulses. However, the detected signal amplitude depends on the nutation angle $\theta = \gamma B_1 t_p$. In order to maintain the optimal value of $\theta \approx 120°$, we must therefore increase B_1, the amplitude of the RF magnetic field. The peak power output of the transmitter increases rapidly with B_1 (as B_1^2), and eventually limits the excitation bandwidth.

Stochastic or "noise" NQR (known as sNQR) has recently been shown to obtain broadband excitation under

peak RF power constraints. The technique uses a long train of short, low-power, and closely-spaced RF pulses with pseudorandomly-varying phases to generate NQR signals [18]. Similar techniques are popular for solid-state NMR spectroscopy [38]. The spectral resolution of sNQR is similar to that of conventional pulsed NQR, and it is useful for locating the precise frequency of a transition once a bandwidth of interest has been identified using a DR method. It can also find lines that are not visible in DR spectra. Examples include lines generated by ^{14}N sites with no nearby protons, and those with T_1 values that are too long or too short to be compatible with sample transfer speeds. Signal amplitudes in sNQR can be used to measure T_1, but are also less sensitive to its precise value. This is a useful property when the value of T_1 is unknown, and suitable wait times between scans have to be chosen. In addition, the pseudorandom sequence can be arbitrarily varied by the spectrometer between scans. *This makes it difficult for the resulting sNQR signals to be replicated by attackers, thus increasing the security of this detection method.*

sNQR experiments require broadband front-end electronics that can generate pulses with fast rise and fall times (allowing rapid pulse repetition rates), and also have short receiver recovery times (allowing rapid signal acquisition). A number of hardware and pulse sequence techniques can be used to reduce receiver recovery time, including preamplifiers that use active, noiseless feedback damping to increase small-signal bandwidth [39], [40], "Q-switch" circuits that use FET switches to dissipate residual energy in the coil [41], and coherent cancellation of the residual energy by using composite pulses [39]. We have recently developed ultra-broadband front-end electronics that are very suitable for both 2D NQR and sNQR [42].

2.6 Imaging

The security of the authentication process can be further enhanced by spatially selective detection, i.e., by imaging the locations of the NQR signal sources. Imaging also allows us to verify that the sample is correctly positioned within the detector, and to study the variability between individual doses (caplets, tablets) in a package, which is often significant for counterfeit medicines [43]. NQR imaging has been demonstrated several times over the last 25 years [44], [45], [46], but has had limited impact because of low measurement sensitivity and spatial resolution. We propose the use of polarization enhancement and advanced image reconstruction algorithms to improve this situation.

A variety of physical mechanisms can be exploited to generate spatially-dependent contrast in NQR signals. For example, orientation-dependent Zeeman shifts in NQR resonance frequencies occur in the presence of a small static magnetic field (B_0) as shown in Fig. 10. Powder samples consist of a large number of randomly-oriented microcrystallites, resulting in randomly-varying shifts, line broadening, and increased relaxation rates [30]. This *relaxation rate contrast mechanism* allows quadrupolar spin density images to be measured by applying a spatially-varying B_0 field across the sample. The zero-field echo decay measured by SLSE (or some other multiple-echo sequence) is often well-modeled by a single exponential, as in Fig. 10. The multi-exponential decay measured in the presence of B_0 can then

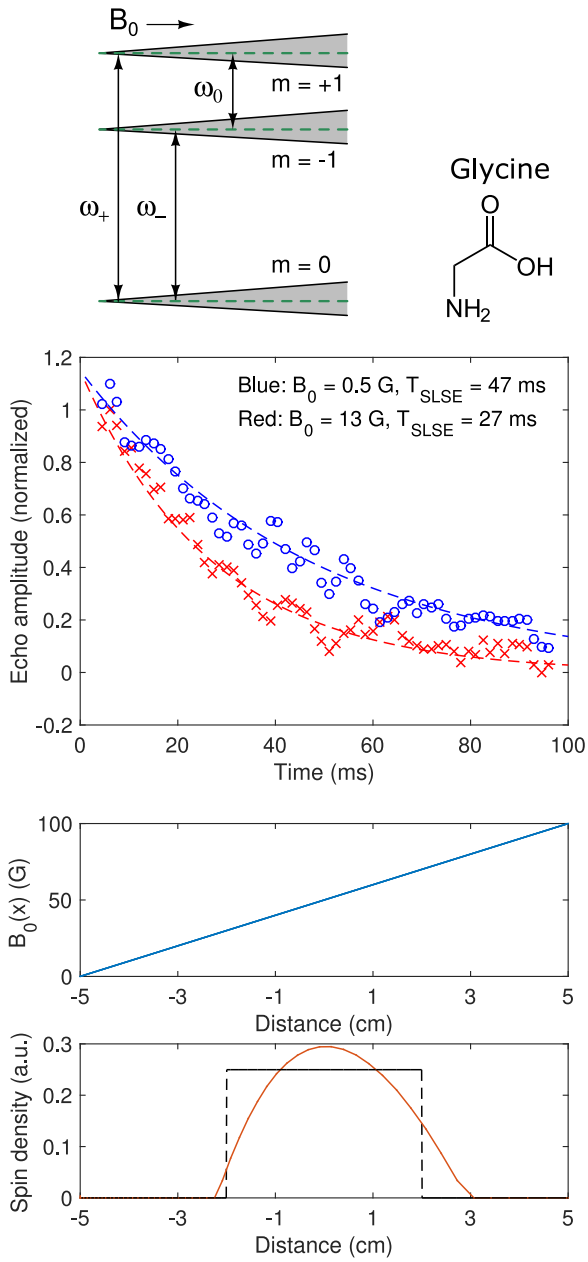

Fig. 10. Top: Zeeman-perturbed NQR energy level diagram for nuclei with spin number $I = 1$. The magnetic field splits each level into a continuous distribution, thus broadening the resonant lines and increasing relaxation rates. Middle: Measured enhancement of the SLSE relaxation rate for the ω_- line of powdered glycine (737 kHz) in the presence of a weak static magnetic field. Bottom: Simulated 1D spin density image of a glycine sample in a constant field gradient $dB_0/dx \equiv g_x = 10$ G/cm. An SNR value of 50 was assumed while performing the inversion.

be converted into a 1D relaxation-time distribution $\rho(R)$ by solving the integral equation $s(t) = \int \rho(R) e^{-Rt} dR$ through the Inverse Laplace Transform (ILT), where $R = 1/T_{SLSE}$ denotes the measured relaxation rate. Efficient numerical techniques exist for solving this inversion problem, which also occurs in the context of NMR relaxometry [47], [48], [49], [50], but regularization must be used to impose desirable constraints such as non-negativity and smoothness. The inverted function $\rho(R)$ is finally converted into a single-shot 1D image $\rho(x)$ of the sample by rescaling the horizontal axis based on the known sensitivity functions $R = f(B_0)$ and $B_0(x)$. An example is shown in Fig. 10.

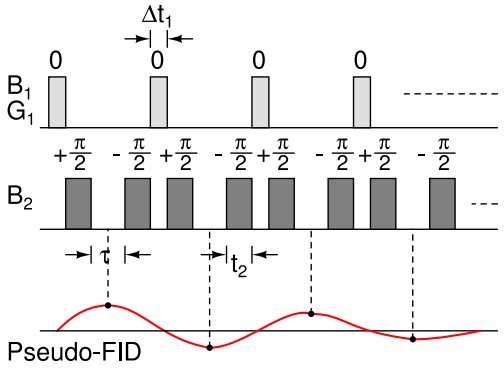

Fig. 11. Pulse sequence for rapid phase-encoded rotating-frame NQR imaging [52]. The B_1 field is accompanied by an RF gradient G_1, while the B_2 field is in the same direction but uniform. The 1D image of the sample is reconstructed by inverting the periodically-sampled signal phase between pulses, which is known as the pseudo-FID (Free Induction Decay).

A more general Zeeman-perturbed NQR imaging technique is to run a series of scans with varying B_0 profiles, and then solving the resulting set of algebraic equations [44]. Accurate, programmable, multi-channel pulsed field gradient (PFG) generators and optimized inversion algorithms are necessary for this type of imaging.

One disadvantage of using Zeeman shifts for imaging is the resulting line broadening, i.e., loss in spectral resolution. This problem is avoided through zero-field rotating-frame NQR imaging (ρ-NQRI), in which spatial information is encoded in B_1 gradients [45], [46], [51]. Accelerated versions of this technique allow 1D images to be acquired within a single scan at the cost of losing spectroscopic information [46]. Phase-encoded ρ-NQRI is known to improve sensitivity and preserve the sign of the spatial coordinate (see Fig. 11), but requires two RF transmitters and coils [52]. Two transmitters and coils are also useful for generating 2D ρ-NQRI images of spin density [53] and the local orientation of the EFG tensor at the quadrupole sites, i.e., molecular orientation in solids [54]. The well-known sensitivity of NQR frequencies and linewidths to temperature, pressure, and internal stress distribution allows these quantities to also be imaged using ρ-NQRI [55]. Thus ρ-NQRI can be used to study aging processes and distinguish between samples of the same API from different manufacturers. However, the spatial resolution is limited by available RF power and the need to use a nonlinear inversion algorithm, such as Fourier deconvolution or the maximum entropy method (MEM). In quadrupolar systems where the nuclear spins do not couple appreciably among themselves, pulsed double resonance imaging (PUDOR or DRI) with quadrupole detection provides higher resolution and a simpler inversion procedure [56]. Multi-channel power-efficient RF transmitters are required to implement both ρ-NQRI and PUDOR-based imaging methods. SNR can be improved by pre-polarizing the sample with a permanent magnet, as described earlier.

2.7 Active Noise Cancellation (ANC)

RFI is a major concern for many NQR applications, as mentioned earlier. In particular, ^{14}N NQR measurements are significantly affected by piezoelectric and magnetoacoustic ringing from metallic objects, ferrites, ferroelectrics, and piezoelectrics, as well as broadcast transmissions in the AM radio band. Passive RFI mitigation methods use specially-designed detectors (coils) with low magnetic dipole moment to reduce interference pickup [57], [58], [59], while active methods use additional "reference" detectors to measure the interference and an adaptive filtering technique to cancel it. Adaptive noise cancellation using multiple reference coils has proven to be vital for surface NMR measurements of groundwater using the Earths magnetic field, where it often increases the final SNR by a factor of 10 or more [60].

Passive cancellation with quadrupolar coils (often known as gradiometers) can significantly reduce RFI pickup and thus eliminate the need for RF shielding in laboratory and field environments, but is always accompanied by some loss of intrinsic detection sensitivity and signal-to-noise ratio. Such problems can be avoided with active noise cancellation (ANC) techniques, which are simple to implement and applicable to all types of RFI (deterministic or stochastic, stationary or time-variable). A multi-channel receiver system allows ANC with one or more reference coils to be implemented for reducing RFI, as shown in Fig. 12. A set of $N \geq 1$ reference coils is used to measure the RFI at different positions and/or orientations. Using more coils is advantageous when there are several noise or interference sources to be canceled [61]. The signals received by the reference coils will usually be correlated, and can either be averaged together or adaptively decorrelated into linearly-independent signals before adaptive filtering. The digital processing unit in the spectrometer can use a variety of adaptation algorithms with different trade-offs between computational efficiency, accuracy, and convergence time, such as least mean square (LMS), recursive least squares (RLS), and projection onto interference subspaces. Users should select the reference sensor configuration, algorithm, and adaptation parameters that are best suited for a given experiment. The detected information can then be used to automatically adapt measurement parameters such as operating frequency, power level, pulse length, and receiver gain. This ability to optimize NQR measurements in real time is important in field applications where the system must operate autonomously, such as authenticating medicines in the rural areas of many LMICs.

3 Experimental Results

In this section we discuss some experimental results. NQR is a volumetric measurement; the signal amplitude is directly proportional to the number of nuclei *of a given type* present within the detector (receiver coil). The first experiment is intended to demonstrate this specific and quantitative relationship. For this purpose, we created and measured several mixtures of two functionally similar medicines: Tylenol (paracetamol) and Aspirin (acetylsalicylic acid). Paracetamol contains a single nitrogen atom and generates NQR signals with resonant frequencies around 2,564, 1,921, and 643 kHz. Aspirin, on the other hand, is one of the few common drugs that do not contain nitrogen and is thus NQR-silent.

This experiment used a single excitation and detection coil that was wound around a hollow PVC cylinder (length = 7.6 cm) with a 6.5 mm high base on both ends. The cylindrical portion had an OD of 3.2 cm and an ID of 1.9 cm. The

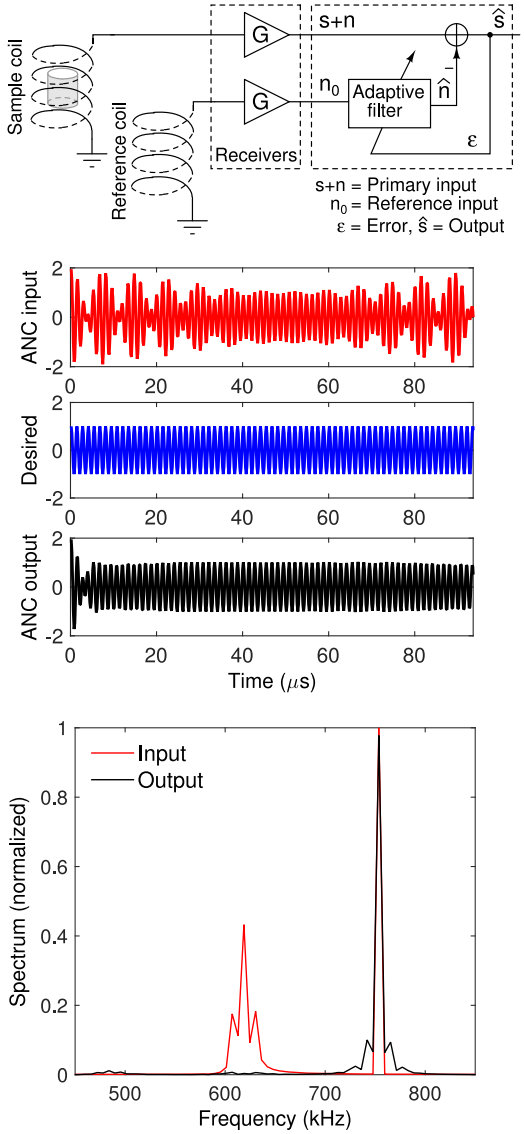

Fig. 12. Top: Simplified block diagram showing active noise cancellation with a single reference input. Bottom: Active cancellation of an amplitude-modulated interferer (carrier frequency = 615 KHz, bandwidth = 10 kHz) from a narrowband NQR signal (center frequency = 750 kHz). The canceler used a 16-stage adaptive FIR filter with weights adjusted using the LMS algorithm.

coil consisted of 20 turns of AWG 18 wire that were wound tightly on the cylinder and then glued in place. The total length of the resulting solenoid was 3.3 cm. It was mounted inside an aluminum box that reduces RFI by acting as a Faraday cage. A maximum of 16 Tylenol caplets (500 mg each) were found to fit inside the coil. We used it to measure NQR spectra around the paracetamol ω_+ line at 2,564 kHz for different numbers of these caplets ($N \leq 16$). In each case, the remaining space within the coil was filled with Aspirin tablets (325 mg each).

Measured results after matched filtering and averaging over eight scans are shown in Fig. 13. They confirm the quantitative nature of NQR. In particular, the measured signal amplitude is directly proportional to the number of Tylenol caplets, i.e., to the volume of active ingredient within the detector. Moreover, the experiment is sensitive enough to reliably detect single Tylenol tablets ($N = 1$).

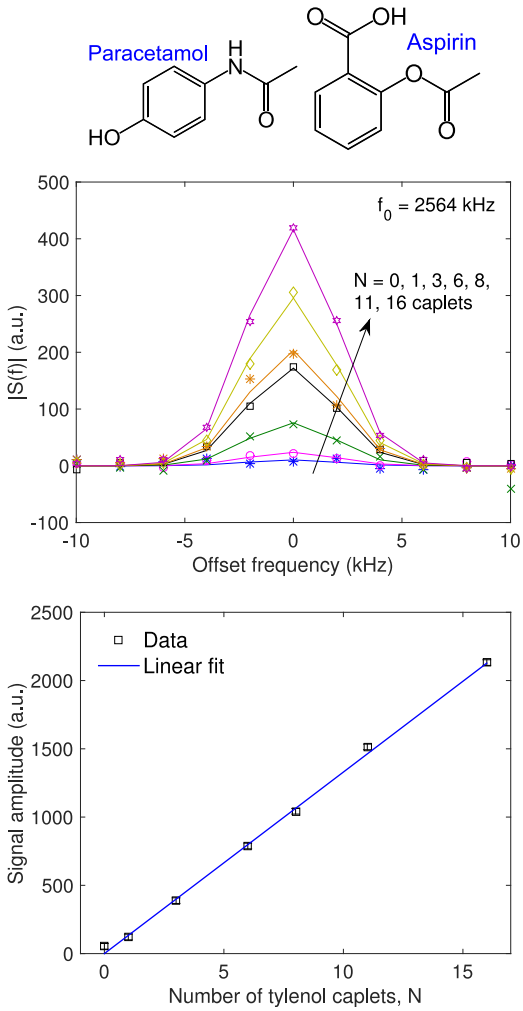

Fig. 13. Top: Measured ^{14}N NQR spectra of a mixture of Tylenol caplets and aspirin tablets around 2.564 MHz. Each spectrum corresponds to a different number of Tylenol caplets within the detector. Each caplet contains 500 mg of the active ingredient (paracetamol, also known as acetaminophen). The data points are averages of eight scans, while the solid lines are Gaussian fits. The total experiment time required for each sample was approximately 30 min. Bottom: Amplitudes of the Gaussian fits shown above as a function of the number of Tylenol caplets.

Fig. 14 shows the results of another experiment. It shows the measured ^{14}N NQR spectra of two falsified medicines: Metakelfin (an anti-malarial) and Orlistat (an anti-obesity drug). Metakelfin pills contain a mixture of two APIs—typically, 500 mg of sulfalene (a sulphonamide antibacterial) and 25 mg of pyrimethamine. The suspect Metakelfin pills, which were labeled as being manufactured by Pfizer in Italy, were collected in Tanzania. They contained only $43 \pm 3\%$ of sulfalene as the genuine article, while the suspect Orlistat pills contained no active ingredient at all. Fig. 14 also shows that the lines from the "suspect" Metakelfin tablets are noticeably narrower than those from the genuine tablets. This result suggests physical differences between the genuine and suspect tablets, such as in the number of defects in the crystal lattice, the processing methods used to make the tablets, and/or the presence of paramagnetic impurities. The manufacturer (Pfizer) later confirmed that the suspect batch was counterfeit, and also provided us with genuine material for comparison.

NQR can be used to authenticate pharmaceuticals that are not essential medicines but are nevertheless susceptible

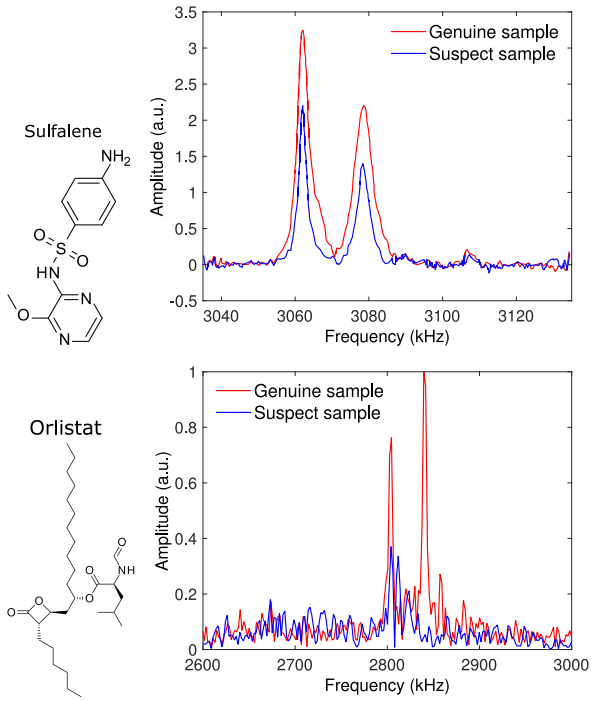

Fig. 14. Two cases of medicines falsification successfully identified using ^{14}N NQR, illustrating that the method is both qualitative and quantitative. Top: Spectra from genuine and suspect Metakelfin pills (red and blue, respectively) in the 3,035-3,135 kHz region, obtained under the same experimental conditions and showing sulfalene peaks at 3,062 and 3,078 kHz [20]. Bottom: Spectra from genuine and suspect Orlistat pills (red and blue respectively) in the 2,600-3,000 kHz region.

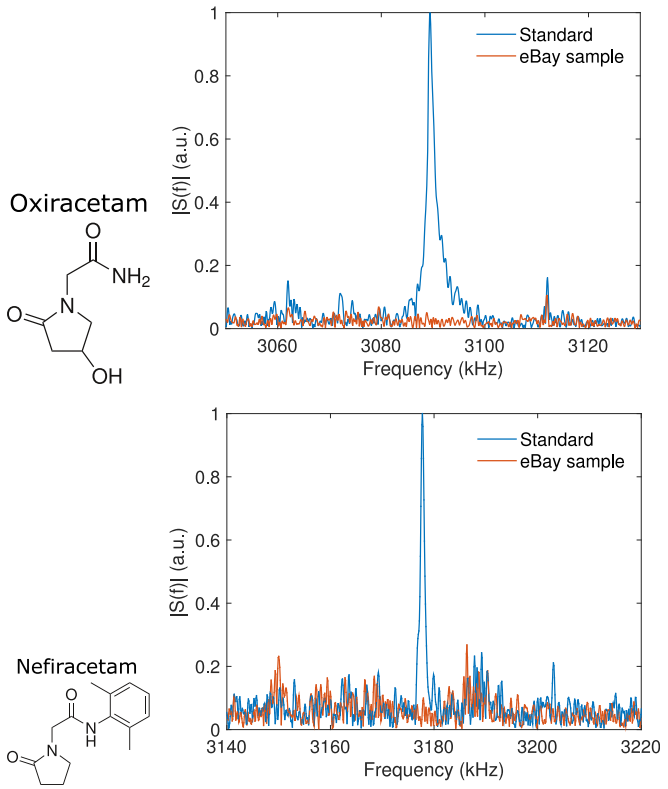

Fig. 15. Two more cases of pharmaceutical falsification successfully identified using ^{14}N NQR. Top: Spectrum of oxiracetam tablets purchased online compared with the genuine compound. Bottom: Similar comparison for nefiracetam tablets.

to counterfeiting. An example is the grey market for so-called cognitive enhancers or smart drugs. Such "nootropic" substances often have unwanted side effects. Some members of the racetam family of drugs (such as piracetam and oxiracetam) are widely consumed as nootropics. Fortunately, these particular drugs have few serious side effects. However, there is also little evidence that they actually enhance cognitive function.

Racetams are chemically defined by the presence of a five-member pyrrolidone ring, which contains nitrogen and is thus NQR-active. We conducted an experiment in which we purchased some oxiracetam and nefiracetam from an online source—specifically, a seller on eBay. These samples were supplied with certificates of analysis, but the measured NQR spectra prove that neither of them actually contains the active ingredient (see Fig. 15). In fact, their ^{1}H NMR spectra were found to match that of myo-inositol, a carbohydrate that is naturally found in many food items and is also widely used as an adulterant (cutting agent) in many illegal drugs.

4 Discussion and Conclusion

We have described a chemometric passport approach for improving the security of the pharmaceutical supply chain. Our approach uses NQR spectroscopy to verify the contents of packaged medicines. Medicines are authenticated by comparing their measured spectra with references stored either on the product barcode or within a secure cloud-based database. We have also described several techniques to increase the robustness of the authentication process, including two-dimensional experiments, polarization enhancements, stochastic excitation, imaging, and active noise cancellation.

NQR provides unique information about the electronic and molecular properties of materials in the solid state. It is similar in many respects to NMR, but does not require an external static magnetic field. This is a key advantage, since the size, weight, and cost of NMR spectrometers are all dominated by their need for a strong and highly homogeneous magnetic field. Even so-called "low-cost" NMR instruments, such as the picoSpin^{TM} (Thermo Scientific) and Spinsolve^{TM} (Magritek), cost $25,000 or more. Optical spectroscopy (Raman, NIR and FTIR) has several advantages including speed, sensitivity, and non-invasiveness, but is similarly limited by the high cost of optical sources and components (lenses, lasers, etc.): Typical portable optical spectrometers cost about $50,000 [7]. By contrast, high-resolution NQR spectra can be readily obtained with miniature instruments that cost less than $250.

Recently developed techniques in the food sciences can be adapted to validate and analyze NQR spectra. For example, high-throughput NMR has been used to identify sources, determine fat and oil content, and provide quality control of dairy products (milk, yogurt, cream, and cheese), fruit juices [62], olive oil, and wines [63]; classification and discrimination information was obtained by comparing a set of spectral features between samples by using multivariate statistics. A similar set of procedures can be used to classify NQR spectra in the presence of experimental errors (incorrect sample placement, temperature drifts, etc.):

1) *Calibration:* Calibration will be used to remove internal and external error sources. An automated sample

motion control system will reduce calibration needs by improving data stability and repeatability.

2) *Data validation:* Automated data quality indicators will be used to reject calibrated spectra that are unsuitable for analysis.
3) *Binning:* Selected spectra will be "binned" by integrating areas of a given size into single data points, which discourages overfitting by reducing the amount of noise.
4) *Integration:* Concentrations of components will be obtained by directly integrating the corresponding lines in each spectrum after deconvolution, or by using statistical methods such as ridge regression.
5) *Classification:* A series of physics-based classification models will be used to validate integrated spectra against known ones in our database. In a hierarchical approach, global models will first be used to determine basic sample properties (such as the components and their concentrations), followed by more specialized models for determining the physical state of the sample, manufacturing process, age, etc. Models will be trained by comparing their predictions for a subset of samples with "ground truth" information from standard laboratory-based analysis methods such as HPLC and MS.

The predictive power of the procedure described above will increase over time as more samples are added to the database and better statistical classification models are introduced. It is also possible to use a model-free or "blind" classification approach that ignores the underlying physics and instead relies entirely on machine learning techniques such as reward-based reinforcement learning (RL). For example, physical properties and composition of complex mixtures (in this case, crude oils at high temperatures and pressures), have been successfully determined by training an artificial neural network on a database of two-dimensional NMR relaxation and diffusion measurements [64]. The model-free approach is applicable to a wider range of different experiments, but typically also exhibits slower learning for complex problems.

We are currently expanding our existing NQR spectral database to enable chemical fingerprinting of medicines and other compounds, such as nutritional supplements. In addition, there is insufficient data on fraud and misrepresentation in pharmaceutical products to direct further research, particularly in LMICs. This gap can be reduced by conducting a set of systematic surveys focused on online drug markets. Specifically, we plan to purchase medicines from a selected group of online sources in various countries and analyze them using NQR-based authentication devices. A subset will be further analyzed with HPLC, MS, X-ray diffraction, or other methods, and the results classified using metrics such as product type, function, cost, country of origin, etc. Such a comprehensive multi-modal database may eventually enable us to move beyond authentication, where the expected composition of the sample is known, to the analysis of unknown mixtures.

Acknowledgments

The authors would like to thank Y.-Q. Song for many interesting discussions on NQR and related topics.

References

[1] United Nations Human Rights Council (UNHRC). Access to medicine in the context of the right of everyone to the enjoyment of the highest attainable standard of physical and mental health, UNHRC resolution A/HRC/RES/12/24, Oct. 2009.
[2] A. I. Wertheimer and J. Norris, "Safeguarding against substandard/counterfeit drugs: Mitigating a macroeconomic pandemic," *Res. Social Administrative Pharmacy*, vol. 5, no. 1, pp. 4–16, 2009.
[3] A. I. Wertheimer and P. G. Wang, *Counterfeit Medicines Volume I: Policy, Economics and Countermeasures*. Hertfordshire, U.K.: ILM Publications, 2012.
[4] P. G. Wang and A. I. Wertheimer, *Counterfeit Medicines Volume II: Detection, Identification and Analysis*. Hertfordshire, U.K.: ILM Publications, 2012.
[5] T. Almuzaini, I. Choonara, and H. Sammons, "Substandard and counterfeit medicines: A systematic review of the literature," *BMJ Open*, vol. 3, no. 8, pp. 1–7, 2013.
[6] H. Kaur, C. Goodman, E. Thompson, K.-A. Thompson, I. Masanja, S. P. Kachur, and S. Abdulla, "A nationwide survey of the quality of antimalarials in retail outlets in Tanzania," *PLoS One*, vol. 3, no. 10, p. e3403, 2008.
[7] S. Kovacs, S. E. Hawes, S. N. Maley, E. Mosites, L. Wong, and A. Stergachis, "Technologies for detecting falsified and substandard drugs in low and middle-income countries," *PloS One*, vol. 9, no. 3, p. e90601, 2014.
[8] J. N. Latosińska, P. Mazurek, and B. Nogaj, "NQR spectroscopy in definition of biological activity of medicines and pesticides," Materials presented at the 27 All-Polish Seminar on Nuclear Magnetic Resonance and its Applications, Cracow, Poland.
[9] S. C. Perez, L. Cerioni, A. E. Wolfenson, S. Faudone, and S. L. Cuffini, "Utilization of pure nuclear quadrupole resonance spectroscopy for the study of pharmaceutical crystal forms," *Int. J. Pharmaceutics*, vol. 298, no. 1, pp. 143–152, 2005.
[10] J. N. Latosińska, "Nuclear Quadrupole Resonance spectroscopy in studies of biologically active molecular systems—A review," *J. Pharmaceutical Biomed. Anal.*, vol. 38, no. 4, pp. 577–587, 2005.
[11] E. Balchin, D. J. Malcolme-Lawes, I. J. F. Poplett, M. D. Rowe, J. A. S. Smith, G. E. S. Pearce, and S. A. C. Wren, "Potential of nuclear quadrupole resonance in pharmaceutical analysis," *Analytical Chemistry*, vol. 77, no. 13, pp. 3925–3930, 2005.
[12] E. Tate, K. Althoefer, J. Barras, M. D. Rowe, J. A. S. Smith, G. E. S. Pearce, and S. A. C. Wren, "Quantitative ^{35}cl nuclear quadrupole resonance in tablets of the antidiabetic medicine Diabinese," *Analytical Chemistry*, vol. 81, no. 13, pp. 5574–5576, 2009.
[13] C. Eliasson and P. Matousek, "Noninvasive authentication of pharmaceutical products through packaging using spatially offset Raman spectroscopy," *Analytical Chemistry*, vol. 79, no. 4, pp. 1696–1701, 2007.
[14] H. Wu, E. J. Heilweil, A. S. Hussain, and M. A. Khan, "Process analytical technology (PAT): Effects of instrumental and compositional variables on terahertz spectral data quality to characterize pharmaceutical materials and tablets," *Int. J. Pharmaceutics*, vol. 343, no. 1, pp. 148–158, 2007.
[15] C. Ricci, L. Nyadong, F. Yang, F. M. Fernandez, C. D. Brown, P. N. Newton, and S. G. Kazarian, "Assessment of Hand-held Raman instrumentation for in situ screening for potentially counterfeit artesunate antimalarial tablets by FT-Raman spectroscopy and direct ionization mass spectrometry," *Analytica Chimica Acta*, vol. 623, no. 2, pp. 178–186, 2008.
[16] M. B. Lopes, J.-C. Wolff, J. M. Bioucas-Dias, and M. A. T. Figueiredo, "Determination of the composition of counterfeit Heptodin^{TM} tablets by near infrared chemical imaging and classical least squares estimation," *Analytica Chimica Acta*, vol. 641, no. 1, pp. 46–51, 2009.
[17] Y. K. Lee, "Spin-1 nuclear quadrupole resonance theory with comparisons to nuclear magnetic resonance," *Concepts Magn. Resonance*, vol. 14, no. 3, pp. 155–171, 2002.
[18] J. Barras, K. Althoefer, M. Rowe, I. Poplett, and J. Smith, "The emerging field of medicines authentication by nuclear quadrupole resonance spectroscopy," *Appl. Magn. Resonance*, vol. 43, no. 4, pp. 511–529, 2012.
[19] J. Barras, A. Jakobsson, E. Gudmundson, M. D. Rowe, I. J. F. Poplett, J. Lužnik, V. Jazbinšek, J. Pirnat, J. Seliger, Z. Trontelj, J. A. S. Smith, and K. Althoefer, "The emerging field of medicines authentication by nuclear quadrupole resonance spectroscopy," in *Counterfeit Medicines Volume II: Detection, Identification and Analysis*, P. Wang and A. I. Wertheimer, Eds. Hertfordshire, U.K.: ILM Publications, 2012.

[20] J. Barras, D. Murnane, K. Althoefer, S. Assi, M. D. Rowe, I. J. F. Poplett, G. Kyriakidou, and J. A. S. Smith, "Nitrogen-14 nuclear quadrupole resonance spectroscopy: A promising analytical methodology for medicines authentication and counterfeit antimalarial analysis," *Analytical Chemistry*, vol. 85, no. 5, pp. 2746–2753, 2013.

[21] J. Lužnik, J. Pirnat, V. Jazbinšek, Z. Lavrič, S. Srčič, and Z. Trontelj, "The influence of pressure in paracetamol tablet compaction on ^{14}N nuclear quadrupole resonance signal," *Appl. Magn. Resonance*, vol. 44, no. 6, pp. 735–743, 2013.

[22] R. Pappu, B. Recht, J. Taylor, and N. Gershenfeld, "Physical one-way functions," *Science*, vol. 297, no. 5589, pp. 2026–2030, 2002.

[23] J. Fraissard and O. Lapina, Eds., *Explosives Detection using Magnetic and Nuclear Resonance Techniques*, series NATO Science for Peace and Security Series B: Physics and Biophysics. New York, NY, USA: Springer, 2009.

[24] S. Somasundaram, A. Jakobsson, M. Rowe, J. Smith, N. Butt, and K. Althoefer, "Robust detection of stochastic nuclear quadrupole resonance signals," *IEEE Trans. Signal Process.*, vol. 56, no. 9, pp. 4221–4229, Sep. 2008.

[25] A. Svensson and A. Jakobsson, "Adaptive detection of a partly known signal corrupted by strong interference," *IEEE Signal Process. Lett.*, vol. 18, no. 12, pp. 729–732, Dec. 2011.

[26] N. R. Butt, E. Gudmundson, and A. Jakobsson, "An overview of NQR signal detection algorithms," in *Magnetic Resonance Detection of Explosives and Illicit Materials*, series NATO Science for Peace and Security Series B: Physics and Biophysics, T. Apih, B. Rameev, G. Mozzhukhin, and J. Barras, Eds. New York, NY, USA: Springer, 2013, pp. 19–34.

[27] S. Mandal and Y.-Q. Song, "Two-dimensional NQR using Ultra-broadband electronics," *J. Magn. Resonance*, vol. 240, pp. 16–23, 2014.

[28] K. L. Sauer, B. H. Suits, A. N. Garroway, and J. B. Miller, "Three-frequency nuclear quadrupole resonance of Spin-1 nuclei," *Chemical Physics Lett.*, vol. 342, pp. 362–368, Jul. 2001.

[29] G. V. Mozzhukhin, B. Z. Rameev, N. Doğan, and B. Aktaş, "The Two-frequency multipulse sequence in nuclear quadrupole resonance of N-14 nuclei," in *Explosives Detection Using Magnetic and Nuclear Resonance Techniques*, 1st ed., J. Fraissard and O. Lapina, Eds. New York, NY, USA: Springer, 2009.

[30] J. Lužnik, V. Jazbinšek, J. Pirnat, J. Seliger, and Z. Trontelj, "Zeeman shift: A tool for assignment of ^{14}N NQR lines of non-equivalent ^{14}N atoms in powder samples," *J. Magn. Resonance*, vol. 212, no. 1, pp. 149–153, 2011.

[31] K. R. Thurber, K. L. Sauer, M. L. Buess, C. A. Klug, and J. B. Miller, "Increasing ^{14}N NQR signal by ^{1}H-^{14}N level crossing with small magnetic fields," *J. Magn. Resonance*, vol. 177, no. 1, pp. 118–128, 2005.

[32] T. Rudakov and P. Hayes, "Cross-polarisation method for improvement of ^{14}N NQR signal detectability," *J. Magn. Resonance*, vol. 183, no. 1, pp. 96–101, 2006.

[33] J. Lužnik, J. Pirnat, V. Jazbinšek, T. Apih, A. Gregorovič, R. Blinc, J. Seliger, and Z. Trontelj, "Polarization enhanced 'single shot' ^{14}N nuclear quadrupole resonance detection of trinitrotoluene at room temperature," *Appl. Phys. Lett.*, vol. 89, no. 12, p. 123509, 2006.

[34] J. Lužnik, J. Pirnat, V. Jazbinšek, Z. Trontelj, T. Apih, A. Gregorovič, R. Blinc, and J. Seliger, "Polarization enhanced NQR detection at low frequencies," in *Explosives Detection Using Magnetic and Nuclear Resonance Techniques*, series NATO Science for Peace and Security Series B: Physics and Biophysics, J. Fraissard and O. Lapina, Eds. New York, NY, USA: Springer, 2009, pp. 41–56.

[35] P. Nath, C. K. Chandrana, D. Dunkerley, J. A. Neal, and D. Platts, "The 'Shim-a-ring' magnet: Configurable static magnetic fields using a ring magnet with a concentric ferromagnetic shim," *Appl. Phys. Lett.*, vol. 102, no. 20, pp. –, 2013.

[36] S. Mandal and Y. Q. Song, "A miniature NMR sensor suitable for High-temperature High-pressure fluid analysis," presented at the Experimental NMR Conf., Boston, MA, USA, Mar. 2014.

[37] F. Noack, "NMR field-cycling spectroscopy: Principles and applications," *Progress Nuclear Magn. Resonance Spectroscopy*, vol. 18, no. 3, pp. 171–276, 1986.

[38] S. L. Wilcke, E. J. Cairns, and J. A. Reimer, "An effective stochastic excitation strategy for finding elusive NMR signals from solids," *Solid State Nuclear Magn. Resonance*, vol. 29, no. 13, pp. 199–203, 2006, special Issue honouring Prof. Alexander Pines on his 60th birthday.

[39] D. I. Hoult, "Fast recovery, high sensitivity NMR probe and pre-amplifier for low frequencies," *Rev. Sci. Instruments*, vol. 50, no. 2, pp. 193–200, 1979.

[40] S. Mandal, M. Hürlimann, and Y. Q. Song, "Optimizing Low-frequency NMR measurements," in *Proc. Magnetic Resonance in Porous Media Conf.*, Wellington, NZ, Feb. 2014.

[41] M. S. Conradi, "FET Q switch for pulsed NMR," *Rev. Sci. Instruments*, vol. 48, no. 3, pp. 359–361, 1977.

[42] S. Mandal, S. Utsuzawa, D. G. Cory, M. D. Hürlimann, M. Poitzsch, and Y.-Q. Song, "An ultra-broadband low-frequency magnetic resonance system," *J. Magn. Resonance*, vol. 242, pp. 113–125, May 2014.

[43] B. J. Venhuis, M. E. Zwaagstra, P. H. J. Keizers, and D. De Kaste, "Dose-to-dose variations with single packages of counterfeit medicines and adulterated dietary supplements as a potential source of false negatives and inaccurate health risk assessments," *J. Pharmaceutical Biomed. Anal.*, vol. 89, pp. 158–165, 2014.

[44] S. Matsui, K. Kose, and T. Inouye, "An NQR imaging experiment on a disordered solid," *J. Magn. Resonance (1969)*, vol. 88, no. 1, pp. 186–191, 1990.

[45] E. Rommel, P. Nickel, R. Kimmich, and D. Pusiol, "Rotating-frame NQR imaging," *J. Magn. Resonance (1969)*, vol. 91, no. 3, pp. 630–636, 1991.

[46] T. M. Osán, L. M. Cerioni, J. Forguez, J. M. Ollá, and D. J. Pusiol, "NQR: From imaging to explosives and drugs detection," *Physica B: Condensed Matter*, vol. 389, no. 1, pp. 45–50, 2007.

[47] G. Goelman and M. Prammer, "The CPMG pulse sequence in strong magnetic field gradients with applications to oil-well logging," *J. Magn. Resonance, Series A*, vol. 113, no. 1, pp. 11–18, 1995.

[48] Y.-Q. Song, L. Venkataramanan, M. Hürlimann, M. Flaum, P. Frulla, and C. Straley, "T_1-T_2 correlation spectra obtained using a fast two-dimensional Laplace inversion," *J. Magn. Resonance*, vol. 154, no. 2, pp. 261–268, 2002.

[49] L. Venkataramanan, Y.-Q. Song, and M. D. Hurlimann, "Solving Fredholm integrals of the first kind with tensor product structure in 2 and 2.5 dimensions," *IEEE Trans. Signal Process.*, vol. 50, no. 5, pp. 1017–1026, May 2002.

[50] M. Hürlimann and L. Venkataramanan, "Quantitative measurement of two-dimensional distribution functions of diffusion and relaxation in grossly inhomogeneous fields," *J. Magn. Resonance*, vol. 157, no. 1, pp. 31–42, 2002.

[51] S. V. Swaminathan and B. Suits, "Reconstructing powder NQR images with real gradient coils," *J. Magn. Resonance*, vol. 138, no. 1, pp. 123–126, 1999.

[52] F. Casanova, H. Robert, and D. Pusiol, "Phase-modulated rotating-frame NQR techniques for spatial encoding," *J. Magn. Resonance*, vol. 141, no. 1, pp. 62–67, 1999.

[53] H. Robert and D. Pusiol, "Two-dimensional rotating-frame NQR imaging," *J. Magn. Resonance*, vol. 127, no. 1, pp. 109–114, 1997.

[54] F. Casanova, H. Robert, and D. Pusiol, "Mapping molecular orientation in solids by rotating-frame NQR techniques," *J. Magn. Resonance*, vol. 133, no. 1, pp. 129–133, 1998.

[55] P. Nickel, H. Robert, R. Kimmich, and D. Pusiol, "NQR method for stress and pressure imaging," *J. Magn. Resonance, Series A*, vol. 111, no. 2, pp. 191–194, 1994.

[56] J. Perlo, F. Casanova, H. Robert, and D. Pusiol, "Solid state proton imaging detected by quadrupole resonance," *J. Magn. Resonance*, vol. 150, no. 2, pp. 132–136, 2001.

[57] B. Suits, A. Garroway, and J. Miller, "Noise-immune coil for unshielded magnetic resonance measurements," *J. Magn. Resonance*, vol. 131, no. 1, pp. 154–158, 1998.

[58] B. Suits, "The noise immunity of gradiometer coils for ^{14}N NQR land mine detection: Practical limitations," *Appl. Magn. Resonance*, vol. 25, nos. 3/4, pp. 371–382, 2004.

[59] A. Peshkovsky, C. Cattena, L. Cerioni, T. Osán, J. Forguez, W. Peresson, and D. Pusiol, "Noise-resilient multi-frequency surface sensor for nuclear quadrupole resonance," *J. Magn. Resonance*, vol. 194, no. 2, pp. 222–229, 2008.

[60] D. O. Walsh, "Multi-channel surface NMR instrumentation and software for 1D/2D groundwater investigations," *J. Appl. Geophys.*, vol. 66, no. 3-4, pp. 140–150, 2008.

[61] B. Widrow, J. Glover, J. R., J. McCool, J. Kaunitz, C. Williams, R. Hearn, J. Zeidler, J. Eugene Dong, and R. Goodlin, "Adaptive noise cancelling: Principles and applications," *Proc. IEEE*, vol. 63, no. 12, pp. 1692–1716, Dec. 1975.

[62] M. Spraul, B. Schütz, E. Humpfer, M. Mörtter, H. Schäfer, S. Koswig, and P. Rinke, "Mixture analysis by NMR as applied to fruit juice quality control," *Magn. Resonance Chemistry*, vol. 47, no. S1, pp. S130–S137, 2009.
[63] R. Godelmann, F. Fang, E. Humpfer, B. Schutz, M. Bansbach, H. Schafer, and M. Spraul, "Targeted and nontargeted wine analysis by ^{1}H NMR spectroscopy combined with multivariate statistical analysis. Differentiation of important parameters: Grape variety, geographical origin, year of vintage," *J. Agricultural Food Chemistry*, vol. 61, no. 23, pp. 5610–5619, 2013.
[64] V. Anand, R. Freedman,et al., "New methods for predicting properties of live oils from NMR," presented at the SPWLA 50th Annu. Logging Symp., The Woodlands, TX, USA, 2009.

Cheng Chen received the BS degree in optics from Fudan University, Shanghai, China, in 2012 and the MS degree with Outstanding Student Award in electrical engineering from Gannon University, Erie, PA, in 2014. He is currently working toward the PhD degree in the EECS Department, Case Western Reserve University, Cleveland, OH. His research interests include magnetic resonance sensors and measurement techniques.

Fengchao Zhang received the BE degree in optoelectronic information engineering from the Huazhong University of Science and Technology, Wuhan, China, in 2012. He is currently working toward the PhD degree in the Department of Electrical Engineering and Computer Science, Case Western Reserve University, Cleveland, OH. His research interests include hardware security, ultra-low-power very large-scale integration design and architecture, nanoelectromechanical systems-based logic devices, circuits, and architectures.

Jamie Barras has many years of experience in the development and application of NQR techniques. He has over 25 publications and patents, and has led research and development projects in the area of the design and trials of portable NQR systems funded by the Wellcome Trust and under the EU FP7 program for the detection of counterfeit medicines in different scenarios. He has extensive experience in the design and construction of computer based detection systems for NQR spectroscopy. He currently leads the NQR Group at Kings College London.

Kaspar Althoefer received the graduate degree in electronic engineering from the University of Technology Aachen, Germany, and the PhD degree in robot motion planning from Kings College London. He is an electronics engineer, leading research on robotics and intelligent systems in the Centre for Robotics Research, Kings College London. He joined the Kings Robotics Group in 1996 as a lecturer. He is currently a professor of robotics and intelligent systems and the head in the Centre for Robotics Research (CoRe). His research focuses on robot autonomy, modeling of tool-environment interaction dynamics, soft robotics, sensing and neuro-fuzzy-based sensor signal classification with applications in robot-assisted minimally invasive surgery, miniaturization of sensing systems for the remote examination of inaccessible spaces such as the heart, intelligent vehicles, and increased autonomy through embedded intelligence. He has authored/coauthored more than 250 peer-reviewed papers and is named inventor on five patent applications. The total research funding awarded to him exceeds £6 Million, including £4.5 Million as Principal Investigator. He is a member of the IEEE.

Swarup Bhunia received the BE (Hons.) degree from Jadavpur University, Kolkata, India, and the MTech degree from the Indian Institute of Technology (IIT), Kharagpur. He received the PhD degree from Purdue University, IN, in 2005. He is currently a professor in the Department of Electrical and Computer Engineering, University of Florida, Gainesville, FL. Earlier, he served as the T. and A. Schroeder associate professor of electrical engineering and computer science at Case Western Reserve University, Cleveland, OH. He has over 10 years of research and development experience with over 200 publications in peer-reviewed journals and premier conferences and four books (three edited) in the area of VLSI design, CAD, and test techniques. His research interests include low power and robust design, hardware security and trust, adaptive nanocomputing, and novel test methodologies. He has worked in the semiconductor industry on RTL synthesis, verification, and low power design for about three years. He received IBM Faculty Award (2013), US National Science Foundation (NSF) Career Development Award (2011), Semiconductor Research Corporation (SRC) Technical Excellence Award (2005), Best Paper Award in International Conference on VLSI Design (VLSI Design 2012), Best Paper Award in International Conference on Computer Design (ICCD 2004), Best Paper Award in Latin American Test Workshop (LATW 2003), and best paper nomination in Asia and South Pacific Design Automation Conference (ASP-DAC 2006) and in Hardware Oriented Test and Security (HOST 2010), nomination for John S. Diekhoff Award, Case Western Reserve University (2010) and SRC Inventor Recognition Award (2009). He has been serving as an associate editor of the *IEEE Transactions on CAD (TCAD)*, *IEEE Transactions on Multi-Scale Computing Systems (TMSCS)*, *ACM Journal of Emerging Technologies (JETC)*, and *Journal of Low Power Electronics (JOLPE)*. He has served as a guest editor of *IEEE Design & Test of Computers* (2010, 2013), *IEEE Computer Magazine* (2016), *IEEE Transaction on CAD* (2015), and *IEEE Journal on Emerging and Selected Topics in Circuits and Systems* (2014). He has served as a co-program chair of IEEE IMS3TW 2011, IEEE NANOARCH 2013, IEEE VDAT 2014, and IEEE HOST 2015, and in the technical program committee of Design Automation Conference (2014-2015), Design Automation and Test in Europe (DATE 2006-2010), Hardware Oriented Trust and Security Symposium (HOST 2008-2010), IEEE/IFIP International Conference on VLSI (VLSI SOC 2008), Test Technology Educational Program (TTEP 2006-2008), International Symposium on Low Power Electronics and Design (ISLPED 2007-2008), IEEE/ACM Symposium on Nanoscale Architectures (NANOARCH 2007-2010), IEEE International Conference on VLSI (ISVLSI 2008-2010), International Conference of VLSI Design as a track chair (2010) and in the program committee of International Online Test Symposium (IOLTS 2005). He has given tutorials on low-power and robust design and test in premier conference including International Test Conferences (ITC 2009), VLSI Test Symposium (VTS 2010), and Design Automation and Test in Europe (DATE 2009). He is a senior member of the IEEE.

Soumyajit Mandal received the BTech degree from the Indian Institute of Technology, Kharagpur, India, in 2002, and the SM and PhD degrees in electrical engineering from the Massachusetts Institute of Technology (MIT), Cambridge, in 2004 and 2009, respectively. He was a research scientist at Schlumberger-Doll Research, Cambridge, MA, from 2010-2014. He is currently an assistant professor in the Department of Electrical Engineering and Computer Science, Case Western Reserve University, Cleveland, OH. His research interests include analog and biological computation, magnetic resonance sensors, low-power analog and RF circuits, and precision instrumentation for various biomedical and sensor interface applications. Dr. Mandal was a recipient of the President of India Gold Medal (2002), and delivered the annual MIT Microsystems Technology Laboratories (MTL) Doctoral Dissertation Seminar in recognition of outstanding research of interest to a broad audience (2009). He has over 50 publications in peer-reviewed journals and premier conferences. He is a senior member of the IEEE.